# Dielectric function of $\alpha$-Sn and its temperature dependence

L. Viña, H. Höchst,* and M. Cardona
*Max-Planck-Institut für Festkörperforschung, Heisenbergstrasse 1, D-7000 Stuttgart 1, Federal Republic of Germany*
(Received 27 July 1984)

The real and imaginary parts of the dielectric function of $\alpha$-Sn in the (1.2—5.6)-eV photon-energy region have been measured at temperatures between 100 and 350 K. Numerically obtained second derivatives of these spectra show distinct structures attributed to $E_1$, $E_1+\Delta_1$, $E_0'$, $E_0'+\Delta_0'$, $E_2$, $E_1'$, $E_1'+\Delta_1'$, and $E_3$ interband critical points. The line shapes of these structures have been fitted to standard theoretical expressions for various types of critical points. The temperature dependence of the critical-point parameters so obtained is presented. The results are compared with other available data and with theoretical calculations based on the band structure of $\alpha$-Sn. Data are also presented for the $\beta$-Sn obtained after heating $\alpha$-Sn to temperatures above 70 °C.

## I. INTRODUCTION

As shown in the preceding paper,[1] ellipsometry[2] is an excellent method for obtaining the dielectric function of semiconductors versus temperature in the visible, near-ir, and near-uv regions. The quality of the data allows several differentiations as a function of photon frequency. From the so-obtained derivative spectra, interband critical points appear clearly. They can be fitted to standard theoretical line shapes. From these fits the various critical-point (CP) parameters (strengths, Lorentzian broadenings, critical energies, and phase shifts) and their temperature dependence can be accurately obtained.

Gray tin ($\alpha$-Sn) is a zero-gap semiconductor with diamond structure whose band structure is similar to that of InSb (see Fig. 1 of Ref. 1).[3,4] The basic differences between the two materials concern the lack of inversion symmetry in InSb (zinc-blende structure) and the zero gap of gray tin due to the reversal of the order of the $5s$ antibonding states and the $5p$ bonding states at the $\Gamma$ point of the Brillouin zone (BZ), which was discovered by Groves and Paul.[5] Experimental work on this interesting material has been hampered by the difficulties in preparing single crystals, due to its transformation into metallic $\beta$-Sn at a temperature of 13 °C (in the bulk).[6] Early experiments were performed on lumpy polycrystalline samples obtained by transforming $\beta$-Sn at temperatures below 13 °C.[7,8] The growth of single crystals by Ewald and Tufte from mercury solution[9] made optical measurements such as ir reflectivity by reflection techniques on growth surfaces possible. Lindquist and Ewald[8] obtained, from ir-reflection measurements, a gap of 0.085 eV, which is now believed to be due to transitions from the $\Gamma_{25'}$ valence band to the $L_1$ conduction-band minimum.[3,4] Cardona and Greenaway[10] found, by means of reflectivity measurements in the (1—6)-eV region, the energies of the $E_1$, $E_1+\Delta_1$, $E_0'$, $E_2$, and $E_1'$ interband critical points. The measured $E_1$ and $E_1+\Delta_1$ energies (1.3 and 1.8 eV) agreed with predictions by Phillips.[11] Other optical measurements on samples grown from the solution followed (reflectivity at oblique incidence,[12,13] electroreflectance,[12,14] resonant Raman scattering[15]). These results showed some discrepancies with each other and with theoretical calculations of the dielectric function,[3,4,13,16] especially concerning the height of the $E_2$ peak in the reflection spectrum. The influence of the poor quality of the crystals on these measurements, with Hg occlusions and an unknown amount of dissolved Hg, remained an open question.[17] Agreement between measured and calculated[3,4,10–14,16,18–25] critical-point energies is, however, generally good.

A new method of growing high-quality $\alpha$-Sn films has been reported recently:[26] films of $\alpha$-Sn up to a thickness of 0.5 $\mu$m were prepared with the molecular-beam-epitaxy technique at room temperature (RT). These films showed a much higher transformation temperature (about 70 °C) than the crystals grown from Hg solution. This temperature depends on the surface orientation and the film thickness, decreasing with increasing thickness.[27] These films are much flatter and have larger areas than the surfaces of samples grown from the mercury solution.[9] Thus they are particularly suitable for ellipsometric measurements. They also have been used to determine the dispersion relations of the valence bands by means of angle-resolved photoemission.[28]

In this paper we report ellipsometric measurements of the dielectric function of $\alpha$-Sn prepared on InSb by the molecular-beam-epitaxy technique.[26] The measurements were performed at several temperatures between 100 and 350 K. Special emphasis was placed on the investigation of the parameters of the observed critical points as a function of temperature. Data were also obtained for films transformed into metallic $\beta$-Sn after heating to 90 °C.

In the following section we will give a short description of the sample preparation and experimental arrangement of the ellipsometer. In Sec. III we present the experimental data. A discussion, comparison with band-structure calculations, and the results of earlier experiments are given in Sec. IV.

## II. EXPERIMENTAL DETAILS

The $\alpha$-Sn sample was a 950-Å-thick film grown on a $7\times7$-mm$^2$ (001)-oriented InSb surface using the

 

molecular-beam-epitaxy technique of Farrow *et al.*[26] The growth, at a typical rate of 2 Å $s^{-1}$ and monitored by reflection high-energy electron diffraction (RHEED), took place under ultrahigh-vacuum conditions ($3\times10^{-10}$ Torr). The cleaness of the film was monitored by photoemission spectroscopy,[28] and there was no indication of surface oxidation. Further details of sample preparation can be found in Refs. 28 and 29. To avoid surface contamination, the $\alpha$-Sn sample was transferred inside a glove bag in an Ar atmosphere into an ultrahigh-vacuum Dewar. The sample was mounted on the cold finger of a liquid-nitrogen cryostat. The temperature was regulated by means of a resistance heater inside a copper holder. Temperature stability was typically $\pm1$ K.

Measurements were taken with an automatic rotating-analyzer ellipsometer. A tungsten quartz-iodine lamp was used in the (1.2—2.3)-eV range; a 75-W short-arc Xe lamp was used for photon energies above 1.8 eV. The light was dispersed by a $\frac{3}{4}$-m Spex single monochromator, and polarized and analyzed with Rochon-quartz prisms. Photomultipliers with S20 and S1 responses were used in combination with the tungsten and Xe lamps, respectively. All measurements were performed at an angle of incidence of 67.5°. Further details concerning the experimental arrangement can be found in Ref. 30.

## III. RESULTS

The complex dielectric function ($\epsilon$) was obtained from the measured ellipsometric angles ($\Psi$ and $\Delta$). The high-vacuum conditions of sample preparation and measurement allow us to use a simple two-phase model[31] to evaluate $\epsilon$ from the complex reflectance ratio. Figure 1 shows the real ($\epsilon_1$) and imaginary ($\epsilon_2$) parts of $\epsilon$ between 1.2 and 5.6 eV at two selected temperatures. Data collected with both multipliers are matched smoothly in the region of overlap. A 10-meV mesh was used for all temperatures. The structures $E_1$, $E_0'$, $E_2$, $E_1'$, and $E_3$ shift to lower energies and broaden with increasing $T$. To obtain the critical-point parameters and resolve the fine structure, we calculate numerically[32] the second-derivative spectra ($d^2\epsilon/d\omega^2$) of the complex dielectric function from our ellipsometric data. The experimental $d^2\epsilon_1/d\omega^2$ (dots) is displayed in Fig. 2, together with the corresponding fits to critical-point line shapes for the real and imaginary parts of the different gaps. Only structure that appeared consistently at different $T$'s is labeled in this figure. The vertical scale in the regions between $E_1+\Delta_1$ and $E_2$ and above the $E_2$ CP is enlarged by a factor of 20. A least-squares procedure, with both $d^2\epsilon_1/d\omega^2$ and $d^2\epsilon_2/d\omega^2$ fitted simultaneously, was used for fits. Two-dimensional (2D) CP line shapes were employed for the $E_1$, $E_1+\Delta_1$, $E_2$, $E_1'$, and $E_1'+\Delta_1'$ singularities. Excitonic effects were taken into account, allowing for a mixture of two CP's;[33] the mixture of a 2D minimum and a saddle point can be written as[34,35]

$$\epsilon\sim C-\ln(E-\omega-i\Gamma)e^{i\phi}\,, \tag{1}$$

where $E$ is the CP energy, $\omega$ is the photon energy, $\Gamma$ is the broadening parameter, and $\phi$ is a phase angle giving the amount of mixture ($\phi=0$ represents a pure minimum and $\phi=\pi/2$ represents a saddle point).

In the case of 3D CP's, the dielectric function can be approximated by[34,35]

$$\epsilon\sim C+i(\omega-E+i\Gamma)^{1/2}e^{i\phi}\,. \tag{2}$$

An $M_0$ CP corresponds to $\phi=0$, an $M_1$ CP to $\phi=\pi/2$. Equation (2) was used to fit the $E_0'$, $E_0'+\Delta_0'$, $\Delta_7^v-\Delta_6^c$, and $E_3$ transitions.

The $E_0'$ and $E_0'+\Delta_0'$ structure were fitted simultaneously: the spin-orbit (SO) splitting ($\Delta_0'$) of 0.3 eV obtained at 100 K was kept fixed in the fit at higher temperatures. The same procedure was used for $E_1'$ and $E_1'+\Delta_1'$ with $\Delta_1'=228$ meV. The $\Delta_7^v-\Delta_6^c$ structure was fitted, together with $E_0'+\Delta_0'$, keeping the parameters obtained previously for $E_0'+\Delta_0'$ fixed.

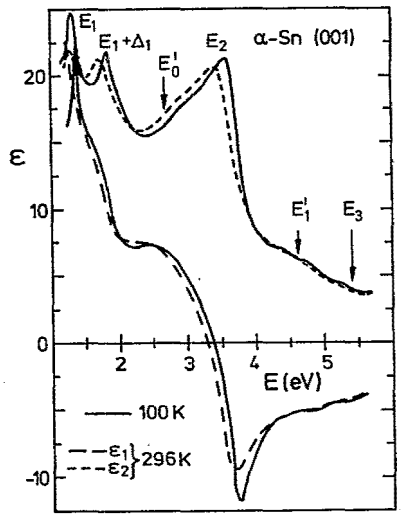


FIG. 1. Real ($\epsilon_1$) and imaginary ($\epsilon_2$) parts of the dielectric function of an $\alpha$-Sn(001) film on InSb at 100 and 296 K.

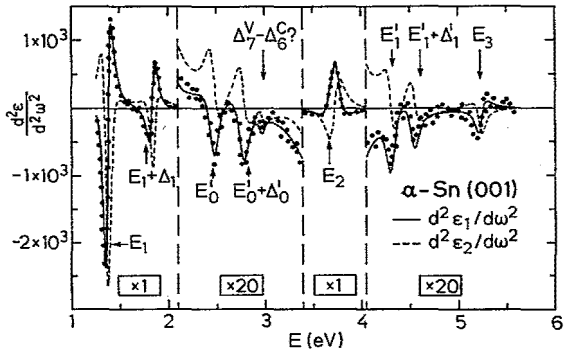


FIG. 2. Experimental second derivatives with respect to the photon energy of the real part of the dielectric function ($d^2\epsilon_1/d\omega^2$) of $\alpha$-Sn at 100 K (dots). Lines correspond to the best fits to the real and imaginary parts with different types of critical points, as explained in the text. The regions corresponding to the $E_0'$ transitions and above the $E_2$ CP are enlarged by a factor of 20. Because of its uncertainty, we have put a question mark on the $\Delta_7^v-\Delta_6^c$ assignment of the structure at 3.0 eV.

TABLE I. Values of the parameters obtained by fitting the critical-point energy ($E$) vs temperature ($T$) to the equations $E(T)=E(0)-\alpha T^2/(\beta+T)$, $E(T)=E_B-\alpha_B[1+2/(e^{\Theta/T}-1)$, and $E(T)=E_L-\gamma T$. Values in parenthesis indicate 95% reliability of the fits. The assignment of the $\Delta_7^v-\Delta_6^c(?)$ structure is uncertain.

| | $E(0)$ (eV) | $\alpha$ ($10^{-4}$ eV K$^{-1}$) | $\beta$ (K) | $E_B$ (eV) | $\alpha_B$ (eV) | $\Theta$ (K) | $E_L$ (eV) | $\gamma$ ($10^{-4}$ eV K$^{-1}$) |
|---|---|---|---|---|---|---|---|---|
| $E_1$ | 1.38(1) | 6(2) | 230(100) | 1.44(4) | 0.09(4) | 340(90) | 1.405(6) | 4.6(3) |
| | | | | | | | | 5.4(6)[a] |
| $E_1+\Delta_1$ | 1.853(5) | 7(4) | 270(140) | 1.97(4) | 0.13(4) | 390(80) | 1.894(7) | 4.9(3) |
| | | | | | | | | 4.2(6)[a] |
| $E_0'$ | | | | | | | 2.51(2) | 4.5(9) |
| | | | | | | | | 1.5(5)[a] |
| $E_0'+\Delta_0'$ | | | | | | | 2.81(2) | 4.5(9) |
| | | | | | | | | ±2[a] |
| $\Delta_7^v-\Delta_6^c(?)$ | | | | | | | 3.02(2) | 5.(1) |
| $E_2$ | 3.748(8) | 7(2) | 220(130) | 3.82(3) | 0.08(3) | 310(90) | 3.780(5) | 5.1(2) |
| | | | | | | | | 3.5(6)[a] |
| $E_1'$ | | | | | | | 4.39(4) | 6.(2) |
| $E_1'+\Delta_1'$ | | | | | | | 4.62(4) | 6.(2) |
| $E_3$ | | | | | | | 5.3(2) | 8.(3) |

[a]Reference 14.

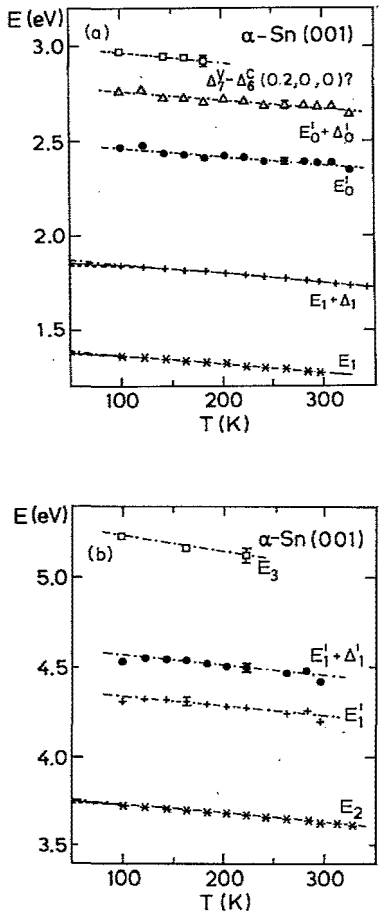


FIG. 3. Dependence on temperature of the critical-point energies of $\alpha$-Sn. Solid lines represent the best fit of the data to Eq. (3), dashed lines, to Eq. (4), and dotted-dashed lines, to Eq. (5).

The critical energies of the analyzed structures are plotted in Figs. 3(a) and 3(b) versus $T$. In Table I we have listed the fit parameters of Varshni's empirical formula,[36]

$$E(T)=E(0)-\frac{\alpha T^2}{T+\beta}\,, \tag{3}$$

and those for an expression proportional to Bose-Einstein statistical factors,[30]

$$E(T)=E_B-\alpha_B\left[1+\frac{2}{e^{\Theta/T}-1}\right], \tag{4}$$

as well as the coefficients of a linear fit,

$$E(T)=E_L-\gamma T\,. \tag{5}$$

The uncertainties in parenthesis in Table I represent 95% reliability.

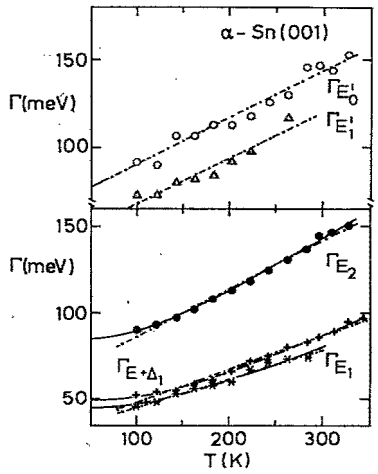


FIG. 4. Dependence on temperature of the critical-point broadening parameters of $\alpha$-Sn. Solid lines represent the best fit to an expression similar to Eq. (4), and dashed lines represent the best linear fit.

TABLE II. Values of the parameters obtained by fitting the Lorentzian broadenings vs temperature to the equations $\Gamma(T)=\Gamma_1+\Gamma_0[1+2/(e^{\Theta/T}-1)]$ and $\Gamma=\Gamma_L+\gamma T$. The temperature $\Theta$ was forced to be the same as in Table I. Values in parenthesis represent 95% reliability of the fits.

| | $\Gamma_L$ (meV) | $\gamma$ ($10^{-4}$ eV K$^{-1}$) | $\Gamma_1$ (meV) | $\Gamma_0$ (meV) | $\Theta$ (K) |
|---|---|---|---|---|---|
| $E_1$ | 28(4) | 1.7(2) | 5(7) | 40(5) | 350 |
| $E_1+\Delta_1$ | 28(4) | 2.0(2) | −2(3) | 51(2) | 390 |
| $E_0'$ | 64(9) | 2.7(4) | | | |
| $E_2$ | 58(4) | 2.7(2) | 31(3) | 53(2) | 310 |
| $E_1'$ | 42(14) | 2.6(8) | | | |

The Lorentzian broadening parameter $\Gamma$ for the $E_1$, $E_1+\Delta_1$, $E_2$, $E_1'$, and $E_0'$ CP's are displayed in Fig. 4 as a function of $T$. The coefficients of the fits to an expression similar to Eq. (4) and a linear expression are represented in Table II. The broadenings of the $E_0'+\Delta_0'$ and $E_1'+\Delta_1'$ CP's are, within the experimental error, equal to those of their spin-orbit-split partners. The error bars for $\Gamma(E_3)$ and $\Gamma(\Delta_7^v-\Delta_6^c)$ are too large to allow us to obtain their temperature dependence.

The phase angles $\phi$ representing the mixture of contiguous CP's are plotted in Fig. 5 versus $T$ for the $E_1+\Delta_1$ and $E_2$ transitions; the values of $\phi$ for the $E_2$ CP of Ge obtained in recent measurements[30] are also displayed for comparison. For $\pi/2<\phi<\pi$, as found from our fit, Eq. (1) represents a mixture of a 2D saddle point with a maximum.

The optical constants of the white-tin film obtained after the phase transition produced by heating to 90 °C are shown in Fig. 6. They display the Drude behavior typical of metals.

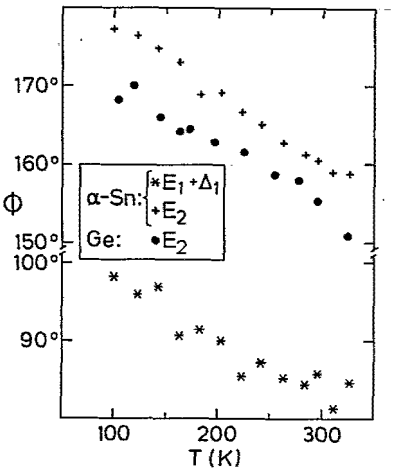


FIG. 5. Dependence on temperature of the excitonic parameter $\phi$ defined in Eq. (1) for the $E_1+\Delta_1$ and $E_2$ CP's of $\alpha$-Sn and for the $E_2$ CP of Ge (dots).

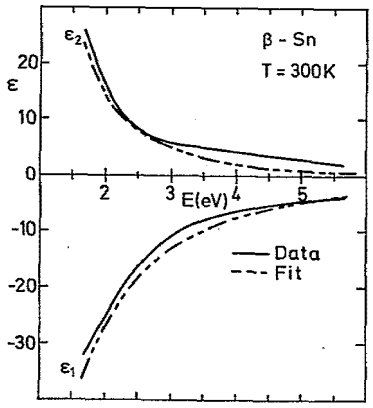


FIG. 6. Pseudodielectric function of the $\beta$-Sn film obtained upon transforming $\alpha$-Sn films by heating to 90 °C measured at RT (solid lines). The dashed lines represent the best fit of the data to Eq. (12).

## IV. DISCUSSION

### A. General

Some comments about the sample conditions are warranted. The carrier concentrations of similarly grown samples have been shown to be lower than $4\times10^{19}$ cm$^{-3}$.[26] Doping below this level has a negligible influence on the transitions studied in this work.[37] The presence of microcrystallites or amorphous $\alpha$-Sn is also ruled out from the measurements of Ref. 27: This would lead, for example, to asymmetric broadening[38] of the Raman line, which has not been observed.[27] Angle-resolved-photoemission experiments[28] indicate that no $\beta$-Sn regions are present in the (001) films below the transition temperature. The lattice constants of $\alpha$-Sn and InSb are[30] 6.4892 and 6.479 37 Å, respectively; as a result of this lattice mismatch, at the interface the $\alpha$-Sn film is laterally compressed, and therefore an elastic dilation along [001] results. The hydrostatic part of this strain should cause a blue shift of the energy gaps,[40] and the uniaxial one leads to a splitting of the energy levels. The last term is usually small and can be neglected. We have estimated the former for the $E_1$ and $E_2$ CP's using the pressure coefficients of these gaps for InSb (Ref. 39) (those of $\alpha$-Sn are not available): blue shifts of 14 and 9 meV are obtained with respect to bulk unstrained $\alpha$-Sn, respectively. These differences should remain nearly constant or slightly decrease with increasing $T$ due to the comparable linear thermal-expansion coefficients of $\alpha$-Sn and InSb ($4.7\times10^{-6}$ and $5.37\times10^{-6}$ K$^{-1}$, respectively[39]).

In Figs. 7(a) and 7(b) the normal-incidence reflectivity spectrum obtained from the measured dielectric function at RT $[R=|(\epsilon^{1/2}-1)/(\epsilon^{1/2}+1)|^2]$ is presented and compared with earlier experimental work and theoretical calculations. Although the agreement in the peak positions in Fig. 7(a) is remarkably good, larger differences are seen in the absolute values of the reflectivity. This fact is probably due to different sample characteristics

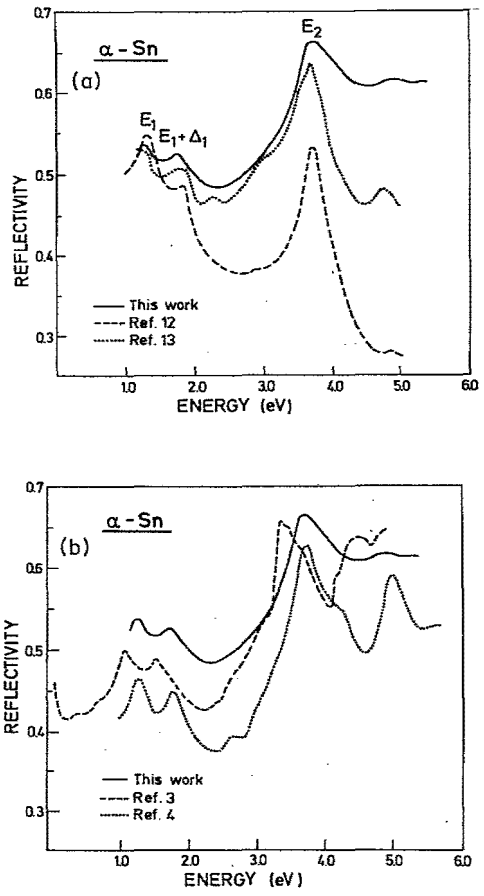


FIG. 7. (a) Normal reflectivity ($R$) spectrum of $\alpha$-Sn at RT from the present work and Refs. 12 and 13. Note the differences in the reflectivity values. (b) Comparison of the present data with calculated reflectivity spectra (Refs. 3 and 4).

and mainly to surface conditions. Typically, the magnitude of the $E_2$ structure and the ratio of the $E_1+\Delta_1$ to $E_1$ peaks decrease if oxides or adsorbed layers are present.[41] In view of the precautions taken to keep the surface clean, and the good agreement with theory (Fig. 7), we believe that the present measurements yield the most reliable optical constants obtained so far for $\alpha$-Sn. In Table III we list the CP energies of the main structures in the optical spectra of $\alpha$-Sn above the fundamental gap taken from the literature, together with the present data. While the best agreement in absolute values of reflectivity with theory is found for the first-principles relativistic orthogonalized-plane-wave calculations of Ref. 3 [Fig. 7(b)], the theoretical critical energies differ in this case by as much as 300 meV from the measured ones. The nonlocal empirical pseudopotential calculations of Ref. 4 obtain CP energies in much better agreement with the present data.

A notable difference between the optical constants of gray Sn and the other two group-IV semiconductors is the magnitude of the $E_2$ peak in $\epsilon_2$ compared with that of the $E_1$ and $E_1+\Delta_1$ CP's, which is much higher in the case of Si (Ref. 37) and Ge (Ref. 30) than for $\alpha$-Sn (see Fig. 1). This observation has also been made in Ref. 12, although in this case the $E_2$ peak is likely to be lowered by surface contamination. We feel that in our case this effect is not due to contamination, but is derived directly from a shift of oscillator strength to lower energies with increasing atomic number. An estimate of the ratio between $\epsilon_2(E_2)$ of Ge and gray tin can be made from the sum rule:[42]

$$n_{\text{eff}}(\omega_M)=\frac{2m}{4\pi^2e^2N_{\text{at}}}\int_0^{\omega_M}\omega'\epsilon_2(\omega')d\omega' = \frac{2m}{4\pi^2e^2N_{\text{at}}}I(\omega_M)\,, \tag{6}$$

TABLE III. Critical-point energies (eV) of interband transitions in gray tin. The corresponding temperatures are given in the footnotes.

| $E_1$ | $E_1+\Delta_1$ | $E_0'$ | $E_0'+\Delta_0'$ | $\Delta_7^v-\Delta_6^c(?)$ | $E_2$ | $E_1'$ | $E_1'+\Delta_1'$ | $E_1'+\Delta_1'+\Delta_1$ | $E_3$ |
|---|---|---|---|---|---|---|---|---|---|
| | | | | Experiment | | | | | |
| 1.28(2)[a] | 1.76(2)[a] | | | | 3.66(2)[a] | | | | |
| 1.25[b] | 1.80[b] | 2.25[b] | | | | | | | |
| 1.25[c] | 1.65[c] | 2.25[c] | | | 3.02[c] | | | | |
| 1.365(2)[d] | 1.845(4)[d] | 2.28[d] | 2.63[d] | | 3.718(2)[d] | 4.11[d] | 4.39[d] | 4.89[d] | |
| 1.316(5)[e] | 1.798(6)[e] | 2.42(3)[e] | 2.72(3)[e] | 2.94(3)[e] | 3.681(4)[e] | 4.28(4)[e] | 4.51(4)[e] | | 5.15(5)[e] |
| | | | | Theory | | | | | |
| 1.10[f] | 1.55[f] | 1.96[f] | 2.45[f] | 2.7[f] | 3.35[f] | 4.2[f] | 4.4[f] | 4.8[f] | 5.4[f] |
| 1.37[g] | 1.45[g] | 2.68[g] | 2.72[g] | 2.94[g] | | | | | |
| 1.33[h] | 1.99[h] | 2.05[h] | 2.75[h] | | 3.77[h] | 4.14[h] | 4.51[h] | 5.17[h] | |
| 1.34[i] | 1.83[i] | 2.08[i] | 2.66[i] | 2.91[i] | 3.78[i] | 4.68[i] | | | |

[a]Reference 10 at 200 K.
[b]From reflectance in Ref. 13 at 278 K.
[c]From $\epsilon$ in Ref. 13 at 278 K.
[d]Reference 14 at 205 K.
[e]This work at 200 K.
[f]Reference 3.
[g]Reference 13.
[h]Reference 25.
[i]Reference 4.

where $N_{at}$ is the atom density and $m(e)$ is the electron mass (charge); the integral

$$I(\omega_M)=\int_0^{\omega_M}\omega'\epsilon_2(\omega')d\omega' \tag{7}$$

is inversely proportional to the atomic volume ($V_{at}$). Using in Eqs. (6) and (7) the approximation $I\simeq\omega(E_2)\epsilon_2(E_2)$, a ratio

$$\frac{[\epsilon_2(E_2)]_{Ge}}{[\epsilon_2(E_2)]_{\alpha\text{-Sn}}}=\frac{[\omega(E_2)V_{at}]_{\alpha\text{-Sn}}}{[\omega(E_2)V_{at}]_{Ge}}=1.3 \tag{8}$$

is obtained. The experimental value of 1.4 for this ratio is in very good agreement with that predicted in Eq. (8).

### B. $E_1$ transitions

The first doublet seen in Fig. 1 below 2 eV corresponds to the structures labeled $E_1$ and $E_1+\Delta_1$. Band-structure calculations localize the transitions responsible for these structures at the $L$ point,[4] or in a region between the point $\vec{k}=(\pi/3a)(1,1,1)$ and the $L$ point,[3] from the upper valence ($\Lambda_{4,5}$) to the lowest conduction bands ($\Lambda_6$) ($E_1$), and from the $\Lambda_6$ valence band to the same conduction band ($E_1+\Delta_1$). A 3D $M_0$ critical point at $L$ and an $M_1$ critical point at $(\pi/24a)(1,1,1)$, with the $M_0$ CP slightly lower in energy, have also been associated with these transitions.[13] The observed line shape is compatible with either a 3D $M_1$ CP or a 2D minimum. The differences between the description of these critical points with either 3D or 2D line shapes has been discussed in detail in Ref. 30. We believe that 2D critical points provide, at present, the most reasonable and internally consistent representation of these transitions.

The second derivatives of the $E_1$ and $E_1+\Delta_1$ structures were fitted simultaneously, allowing for excitonic effects with a mixture of a 2D minimum and a saddle point [Eq. (1)]. The best fit of $d^2\epsilon/d\omega^2$, together with the experimental data for the real part of the dielectric function at 100 K, are shown in Fig. 2. The CP energy of the $E_1$ transition found in the present work (see Table III) is $\sim$50 meV higher than the values obtained with reflectance,[10,13] and the same amount lower than the electroreflectance results.[14] Taking into account the influence of the InSb substrate (see Sec. IV A) brings the discrepancy to $\sim$40 meV with the former results and $\sim$60 meV with the latter results. Line-shape effects are known to be responsible for the discrepancies between peaks in $\Delta R/R$ and in $\Delta\epsilon_1$ and $\Delta\epsilon_2$);[30,43] therefore, we believe that our complete line-shape analysis of the CP's should give the most reliable results. Except for Ref. 3, theoretical values of the $E_1$ and $E_1+\Delta_1$ energies are only slightly higher ($\sim$20 meV) than the present results. The SO splitting $\Delta_1=482\pm6$ meV found in our study agrees reasonably well with previous experimental values and rather well with theoretical values, with the exception of the self-consistent nonlocal pseudopotential calculations of Ref. 25 (see Table IV). This SO splitting remains constant at all temperatures with an uncertainty no larger than the experimental error ($\pm6$ meV).

The broadening parameters of $E_1$ and $E_1+\Delta_1$ are shown in the lower part of Fig. 4 versus $T$. The dotted-dashed lines correspond to the best linear fit, and the solid lines correspond to an equation similar to Eq. (4) where $\Theta$ has been forced to have the same values as for the fit to the corresponding CP energies. The parameters of the fits are listed in Table II. Our values at 100 K, $\Gamma(E_1)=45\pm4$ meV and $\Gamma(E_1+\Delta_1)=52\pm7$ meV, are comparable to those found for Ge,[30] $41\pm3$ and $55\pm7$ meV. As in many other zinc-blende materials,[44] the $E_1+\Delta_1$ structure is slightly broader than the $E_1$ structure.

These structures are known to be strongly affected by excitonic effects, i.e., electron-hole Coulomb interaction.[45] These effects can be described as the interference of a discrete two-dimensional exciton with a quasicontinuous background.[46] A qualitative description can also be effected by multiplying the one-electron $\epsilon$ by a phase factor, as in Eqs. (1) and (2). The phase angle $\phi$, plotted in Fig. 5 for the $E_1+\Delta_1$ CP, decreases rapidly with increasing $T$, indicating a decrease of excitonic effects as $T$ is raised. The value of $\phi=98°$ found at 100 K formally corresponds to a slight mixture of a 2D maximum with a saddle point. This angle increases through the sequence Si, Ge, $\alpha$-Sn, InSb.[1,30,37]

The amplitudes of 2D CP's can be calculated within the one-electron model of Ref. 47:

$$A_{E_1}=44\frac{E_1+\Delta_1/3}{a_0E_1^2}\,, \tag{9a}$$

$$A_{E_1+\Delta_1}=44\frac{E_1+2\Delta_1/3}{a_0(E_1+\Delta_1)^2}\,, \tag{9b}$$

TABLE IV. Spin-orbit splittings (in meV) at different points of the BZ in gray tin.

| $\Delta_1$ | $\Delta_0'$ | $\Delta_1'$ |
|---|---|---|
| | Experiment | |
| 475(30)[a] | | |
| 550[b] | | |
| 400[c] | | |
| 520[d] | 350[d] | 280[d] |
| 482(6)[e] | 300(30)[e] | 228(40)[e] |
| | Theory | |
| 450[f] | 480[f] | 210[f] |
| | 540[g] | |
| 480[h] | 430[h] | 190[h] |
| 660[i] | 700[i] | 370[i] |
| 480[j] | 580[j] | 290[j] |

[a]Reference 10.
[b]Reference 13 (from $R$).
[c]Reference 13 (from $\epsilon$).
[d]Reference 14.
[e]This work.
[f]Reference 3.
[g]G. G. Wepfer, T. C. Collins, and R. N. Euwema, Phys. Rev. B 4, 1296 (1971).
[h]Reference 21.
[i]Reference 25.
[j]Reference 4.

where $a_0$ is the lattice constant in Å, and the energies are in eV. Using the lattice constant of Ref. 39 and the experimental energies of our present work at 100 K, Eqs. (9) predict $A_{E_1}=5.6$ and $A_{E_1+\Delta_1}=3.4$, with a ratio $A_{E_1}/A_{E_1+\Delta_1}=1.6$. Experimentally, $A_{E_1}=7.1$ and $A_{E_1+\Delta_1}=2.5$ are found at 100 K. The agreement is reasonable in view of the crudeness of the theory used. Discrepancies are believed to be due to linear terms in $k$,[48,49] which increase the transverse mass for the $E_1$ gap and decrease it for the $E_1+\Delta_1$ gap, and to an excitonic interaction which increases the amplitude of the $E_1$ structure compared with one-electron calculations.[50] The first contribution is expected to be small in the case of gray tin because of its large SO splitting $\Delta_1$; the latter seems to dominate, as confirmed by the fact that the ratio $A_{E_1}/A_{E_1+\Delta_1}$ decreases from a value of 2.8 at 100 K to 2 at 300 K, where excitonic effects have diminished.

The solid lines of Fig. 3(a) correspond to the best fit to Eq. (3).[36] The parameters of the fit are listed in Table I. $\beta$ should be close to the Debye temperature ($\Theta_D$).[36] Thus, $\beta$ is found to decrease through the sequence Ge, $\alpha$-Sn, InSb,[1,30] following the values of $\Theta_D$.[39] An equally good fit can also be obtained with Eq. (4), which takes into account average statistical factors for absorption and emission of phonons. A similar expression has been used for the fundamental gaps of diamond, silicon, and germanium.[51] Best fits are shown in Fig. 3(a) as dashed lines; fit parameters are listed in Table I. Both fits are equally good; the differences begin at temperatures lower than our experimental ones. Measurements at liquid-He temperatures should decide which of the models yields the best description. The dotted-dashed lines represent a linear fit, and the linear coefficients (Table I) agree within error with those of Ref. 14.

### C. $E_0'$ transitions

$E_0'$ transitions are believed to take place at the $\Gamma$ point, or in the $\Delta$ direction near the $\Gamma$ point[3,4,43] between the $\Gamma_{25'}$ valence bands and the $\Gamma_{15}$ conduction bands. Four structures are expected for these transitions: $E_0'(\Gamma_8-\Gamma_6)$, $E_0'+\Delta_0'(\Gamma_8-\Gamma_8)$, $E_0'+\Delta_0(\Gamma_7-\Gamma_6)$, and $E_0'+\Delta_0'+\Delta_0(\Gamma_7-\Gamma_8)$, with $\Delta_0$ ($\Delta_0'$) the SO splitting of the valence (conduction) band at $\Gamma$. The corresponding critical points have a 3D $M_0$ character.[4] The $E_0'+\Delta_0$ transitions are symmetry forbidden.

The dielectric function for a 3D CP can be approximately described by[47]

$$\epsilon_2=\frac{2}{3\omega^2}(2\mu^{3/2}\Pi^2)(\omega-E_g)^{1/2}=A(\omega-E_g)^{1/2}\,, \quad (10)$$

where $\mu$ is the reduced effective mass of the transitions and $\Pi$ is the corresponding matrix element of $\vec{p}$. The effective masses of the valence $\Gamma_{25'}$ bands and the conduction $\Gamma_{15}$ bands can be obtained from[25]

$$\frac{2m^*E}{\hbar}=\begin{cases} ak^2\pm[b^2k^4+c^2(k_x^2k_y^2+k_y^2k_z^2+k_z^2k_x^2)]^{1/2}, & \text{(11a)} \\ a'k^2-\Delta\,, & \text{(11b)} \end{cases}$$

where $\Delta=\Delta_0$ for the valence bands and $\Delta_0'$ for the conduction bands. The parameters $a$, $b$, $c^2$, and $a'$ can be calculated from the experimental energy gaps and the matrix elements of $\vec{p}$ between $\Gamma_{15}$ and $\Gamma_1,\Gamma_{25'}$ for the conduction band, and $\Gamma_{25'}$ and $\Gamma_{2'},\Gamma_{15},\Gamma_{12'}$ for the valence band.[3,53,54] Using the matrix elements of Ref. 3, we calculate, for the strength $A$ of the CP's, $A_{E_0'}=3.57$,

$$A_{E_0'+\Delta_0'}=1.94,\ A_{E_0+\Delta_0}=0,\text{ and } A_{E_0'+\Delta_0+\Delta_0'}=0.3.$$

We have been able to resolve the $E_0'$ and $E_0'+\Delta_0'$ CP's; the $E_0'+\Delta_0+\Delta_0'$ CP should be very close to $E_2$, and thus too weak to be observed. Line-shape analysis with 3D CP's [see Eq. (2)] yields the following amplitudes, $A_{E_0'}=4.27$ and $A_{E_0'+\Delta_0'}=3$, in qualitative agreement with the above predictions. Contributions of transitions slightly away from the $\Gamma$ point could be responsible for the enhancement of the $E_0'+\Delta_0'$ structure. Our CP energies are about 0.2 eV larger for $E_0'$ than in previous work (see Table III). $E_0'+\Delta_0'$ is also 90 meV larger than the electroreflectance result.[14] Our $\Delta_0'=300\pm30$ meV is in good agreement with electroreflectance[14] and smaller than all theoretical values.

We have assumed $\Delta_0'$ to be $T$ independent and have used the value obtained at 100 K as a fixed parameter while $E_0'$ and $E_0'+\Delta_0'$ were fitted simultaneously. The best fit at 100 K is seen in Fig. 2. Owing to the large scattering in the data, attempts to fit temperature dependences to Eqs. (3) and (4) give parameters without physical meaning. Therefore only a linear fit was performed [Fig. 3(a)]. The $T$-linear coefficients are reported in Table I. The average linear coefficient of $E_0'$ and $E_0'+\Delta_0'$ is found to be comparable to that of the $E_1$ transitions, but is a factor of 3 larger than that found from electroreflectance;[14] it is also larger than that in the case of Ge.[30] The temperature dependence of the broadening parameter is shown in the upper part of Fig. 4 for $E_0'$. The results are similar for the $E_0'+\Delta_0'$ CP. The large scatter in the data allows us to obtain only its linear coefficient (Fig. 4 and Table II), which is somewhat larger than for the $E_1$ transitions.

### D. $E_2$ transition

The $E_2$ transition has the contributions of several critical points. It has been associated with $X_4$-$X_1$ transitions,[10] transitions between the upper valence and lower conduction bands in an extended region near $U$ in the $XUK$ plane,[3,13] and also with a plateau in the transition energy near $(2\pi/a)(0.75, 0.25, 0.25)$.[4] The best fit to this structure was obtained via a mixture of a 2D maximum and a saddle point; this representation also yields the best fit in the case of Ge.[30] The best fit for $\alpha$-Sn can be seen in Fig. 2. In Fig. 5 we have displayed the phase angle $\phi$ [Eq. (1)] versus $T$, together with that of Ge. These $\phi$-vs-$T$ plots show a similar behavior, decreasing with increasing $T$, as for the $E_1$ transitions. This could indicate that excitonic effects are also important for $E_2$, although different temperature shifts of electronic states contributing to this transition cannot be ruled out as the cause of this dependence. The CP energies and broadening parameters versus $T$ are shown in Figs. 3(b) and 4. The lines

represent the best fits with Eqs. (3)—(5). The fit parameters are listed in Tables I and II. For the energy shift they are similar to those of the lower transitions. The effect of $T$ on the broadening is comparable to that of $E_0'$, but larger than that for the $E_1$ transitions, as in the case of Ge.[30] The CP energies at 200 K compare well with previous experimental and theoretical work (see Table III).

### E. $E_1'$ transitions

The next structure above the $E_2$ CP is believed to correspond to transitions between the $L_3$ valence- and $L_3'$ conduction-band doublets. Four structures, labeled $E_1'(L_{4,5}^+ \rightarrow L_6^-)$, $E_1'+\Delta_1'(L_{4,5}^+ \rightarrow L_{4,5}^-)$, $E_1'+\Delta_1(L_6^+ \rightarrow L_6^-)$, and $E_1'+\Delta_1'(L_6^+ \rightarrow L_{4,5}^-)$, should be observed; $\Delta_1(\Delta_1')$ is the SO splitting of the $L_3$ ($L_3'$) band. If these transitions take place at the $L$ point, the $E_1'$ and $E_1'+\Delta_1'+\Delta_1$ structures should be the larger ones, because they are determined by $p_\perp$ matrix elements, while the $E_1'+\Delta_1'$ and the $E_1'+\Delta_1$ structures are determined by $p_{\bar{z}}$ matrix elements (the $\bar{z}$ are the $\{111\}$ directions, and $\perp$ means perpendicular to $\bar{z}$). In the case of Ge (see Fig. 15 of Ref. 54), the former should be an order of magnitude larger than the latter. Full band-structure calculations[3] show, however, two doublets in the (4—5)-eV region: the intensity of the first doublet is almost twice as large as the second. This fact is in agreement with our experiments, although we only have been able to resolve the first doublet. Owing to its energy separation, we have assigned it to the $E_1'$ and $E_1'+\Delta_1'$ transitions. A possible explanation for the discrepancy between experiment and the simple two-band model can be the effect of the $k$-linear coupling on these transitions, as discussed for GaAs in Ref. 49. Critical points could appear in directions perpendicular to the [111] symmetry axis close to the $L$ point (Fig. 1 of Ref. 49) (also see the discussion in Sec. IV F).

We have analyzed these structures with 2D line shapes. The SO splitting $\Delta_1'=228\pm40$ meV found at 100 K was kept constant for the rest of the fits. The CP energies and broadening parameters are shown versus $T$ in Figs. 3(b) and 4. The broadening parameter of the $E_1'+\Delta_1'$ structure is, within experimental error, equal to that of the $E_1'$ structure. The linear coefficients of the CP energies are slightly larger than those of the lower transitions (see Table I). That of $\Gamma$ is, within experimental accuracy, comparable to those of the other transitions. The value of $\Delta_1'$ quoted in Table IV should be taken with care due to the fact that these transitions could correspond to points lying away from the $\{111\}$ directions.[49]

### F. Other transitions

Two more structures are still seen in Fig. 2. The small one above the $E_0'+\Delta_0'$ transition at 2.94 eV may correspond to transitions between the second valence band and the lowest conduction band in the [100] direction. Therefore we have labeled it $\Delta_7^v-\Delta_6^c$. It has been theoretically predicted.[4] However, it has not seen experimentally before. We have been able to resolve it up to 180 K. We have fitted it together with the $E_0'+\Delta_0'$ structure, keeping the parameters obtained before for this CP fixed. Its $T$ dependence is shown in Fig. 3(a). The parameters of the linear fit, comparable to those of $E_2$, are listed in Table I.

We have labeled the highest transition seen in Fig. 2, at about 5.2 eV, $E_3$, as it corresponds, within 0.2 eV, to the theoretically predicted $E_3$ structure (transitions in the $\Gamma XUK$ plane between the upper valence and the third conduction bands).[16] We did not assign it to the $E_1'+\Delta_1'+\Delta_1$ structure because it would lead to a $\Delta_1$ value too large compared to that obtained from the $E_1$ and $E_1+\Delta_1$ CP's. However, if the $k$-linear terms are important, this last possibility should not be disregarded, due to the increase of apparent SO splitting in directions perpendicular to $\{111\}$.[49] Its linear coefficient, larger than that for the other structures but comparable within error, is listed in Table I. The $E_3$ energies are plotted in Fig. 3(b) versus $T$. This is also the first time that this structure has been resolved.

### G. White tin

The optical constants of evaporated white-tin films have been measured by near-normal-incidence reflectance[55] in the energy region from 2.1 to 14.5 eV, and the refraction index from 14.5 to 20.5 eV, by the critical-angle method.[55] Several authors have also measured the optical constants in the infrared region.[56–58] Band-structure calculations are also available in the literature.[59]

In Fig. 6 we presented the optical constants of the tin film measured at RT after the phase transition took place at $\sim$90 °C; this transition temperature agrees well with Raman studies.[27] The phase transition could be monitored by measuring $\epsilon$ at the $E_2$ energy; it produced a large change at this energy (see Figs. 1 and 6). The $\epsilon$'s stabilized about 15 min after the transition. We thus assumed that the transformation was complete. The sample was taken to RT and the $\epsilon$ spectra were measured. The optical constants of the $\beta$-Sn film may be influenced by the fact that microcracks, due to the increased density of $\beta$-Sn, and a rough surface, are formed after the transformation.[26] However, a reasonably good agreement is found with the data of Ref. 55. We have fitted our results with a Drude expression,[42]

$$\epsilon(\omega)=1-\frac{\omega_p^2}{\omega(\omega+i/\tau)} . \tag{12}$$

We obtained, from the fit, $\omega_p=12\pm0.1$ eV and $\tau=(4.1\pm0.5)\times10^{-15}$ s. The fitted curves are plotted as dashed lines in Fig. 6. The deviations between the fit and experimental data are due to interband transitions[55] at about 1.2 eV, unfortunately outside our energy range. Nevertheless, the it is quite good. The energy-independent relaxation time compares well with the value $\tau=4.2\times10^{-15}$ s of Ref. 55. The plasma frequency is high compared with the value, 8.16 eV, obtained from optical data in the far-infrared region (0—0.1 eV).[55] An effective number of electrons, $n_{\text{eff}}=2.82$, is obtained from $\omega_p$, instead of 1.33 in Ref. 55. Our value agrees with $n_{\text{eff}}=2.74$ found for $\alpha$-Sn in the same energy range.

After a period of about 24 h, the $\beta$-Sn film again transforms partially into $\alpha$-Sn. Once the $\alpha$-$\beta$ transition has taken place, $\beta$-Sn seems to prevent the full transformation into $\alpha$-Sn at RT. Thus the transformation is only partly reversible.

## V. CONCLUSIONS

We have measured the effect of temperature on optical interband transitions of gray tin between 1.2 and 5.6 eV. Special care was taken with sample preparation and to avoid surface contamination; this allowed us to obtain reliable optical constants for this material. Real and imaginary parts of the dielectric function are presented in the range 100—350 K. Line-shape analysis of numerically calculated second-derivative spectra of the original data yields information about critical-point energies, broadening parameters, amplitudes, and phases of the $E_1$, $E_0'$, $E_2$, $E_1'$, and $E_3$ structures, and their corresponding SO-split counterparts. Our results compare reasonably well with available band-structure calculations. To free-electron-like optical constants of the white-tin film obtained after the phase transition induced by heating are well described by a Drude model.

## ACKNOWLEDGMENTS

We would like to thank M. Bleder and A. Birkner for help with the construction of the ellipsometer, I. Hernández-Calderón for his assistance in the sample preparation, and W. Neu for expert technical help.

*Present address: Department of Physics, University of Wisconsin, 1150 University Avenue, Madison, Wisconsin 53706.

[1]S. Logothetidis, L. Viña, and M. Cardona, preceding paper, Phys. Rev. B 31, 947 (1985), and references therein.
[2]D. E. Aspnes, Opt. Commun. 8, 222 (1973); D. E. Aspnes and A. A. Studna, Appl. Opt. 14, 220 (1975).
[3]F. H. Pollak, M. Cardona, C. W. Higginbotham, F. Herman, and J. P. Van Dyke, Phys. Rev. B 2, 352 (1970).
[4]J. R. Chelikowsky and M. L. Cohen, Phys. Rev. B 14, 556 (1976).
[5]S. Groves and W. Paul, Phys. Rev. Lett. 11, 194 (1963); in *Proceedings of the 7th International Conference on the Physics of Semiconductors,* edited by M. Balkanski (Dunod, Paris, 1964), p. 41.
[6]O. L. Erdman, J. Pract. Chem. 52, 428 (1951). This phase transition is also obtained for Si and Ge at high pressures.
[7]G. Busch and J. Wieland, Helv. Phys. Acta 26, 697 (1953); G. Busch and R. Kern, in *Solid State Physics,* edited by F. Seitz and D. Turnbull (Academic, New York, 1960), Vol. 11, p. 1.
[8]R. E. Lindquist and A. W. Ewald, Phys. Rev. 135, A191 (1964).
[9]A. W. Ewald and O. N. Tufte, J. Appl. Phys. 29, 1007 (1958).
[10]M. Cardona and D. L. Greenaway, Phys. Rev. 125, 1291 (1962).
[11]J. C. Phillips, Phys. Rev. 125, 1931 (1962).
[12]P. T. McElroy, Technical Report No. HP-21 (ARPA-34), Division of Engineering and Applied Physics, Harvard University, 1968 (unpublished).
[13]T. Hanyu, J. Phys. Soc. Jpn. 31, 1738 (1971).
[14]M. Cardona, P. T. McElroy, F. H. Pollak, and K. L. Shaklee, Solid State Commun. 4, 319 (1966).
[15]M. Iliev, M. Sinyukov, and M. Cardona, Phys. Rev. B 16, 5350 (1977).
[16]C. W. Higginbotham, F. H. Pollak, and M. Cardona, Solid State Commun. 5, 513 (1967).
[17]C. H. L. Goodman, Proc. Inst. Elect. Eng., Part I, 129, 189 (1982).
[18]F. Bassani and L. Liu, Phys. Rev. 132, 2047 (1963).
[19]M. L. Cohen and T. K. Bergstresser, Phys. Rev. 141, 789 (1966).
[20]F. Herman, R. L. Kortum, C. D. Kuglin, and R. A. Short, in *Quantum Theory of Atoms, Molecules, and the Solid State,* edited by P. O. Löwdin (Academic, New York, 1966), p. 381.
[21]S. Bloom and T. K. Bergstresser, Solid State Commun 6, 461 (1968).
[22]M. Nishida, J. Chem. Phys. 69, 956 (1978).
[23]M. Averous, Phys. Status Solidi B 95, 91 (1979).
[24]D. R. Mašović and S. Zeković, Phys. Status Solidi B 96, 469 (1979).
[25]G. P. Srivastava, J. Phys. C 15, 707 (1982); 16, 1649 (1983).
[26]R. F. C. Farrow, D. S. Robertson, G. M. Williams, A. G. Cullis, G. R. Jones, I. M. Young, and M. J. Dennis, J. Cryst. Growth 54, 507 (1981).
[27]J. Menéndez and H. Höchst, Thin Solid Films 111, 375 (1984).
[28]H. Höchst and I. Hernández-Calderón, Surf. Sci. 126, 25 (1983).
[29]I. Hernández-Calderón and H. Höchst, Phys. Rev. B 27, 4961 (1983).
[30]L. Viña, S. Logothetidis, and M. Cardona, Phys. Rev. B 30, 1979 (1984).
[31]N. M. Bashara and R. M. Azzam, in *Ellipsometry and Polarized Light* (North-Holland, Amsterdam, 1977).
[32]A. Savitzky and J. E. Golay, Anal. Chem. 36, 1627 (1974); J. Sternier, Y. Termonia, and J. Deltour, *ibid.* 44, 1906 (1972).
[33]Y. Toyozawa, M. Inoue, T. Inui, M. Okazaki, and E. Hanamura, J. Phys. Soc. Jpn. Suppl. 21, 133 (1967).
[34]M. Cardona, in *Modulation Spectroscopy,* Supplement 11 of *Solid State Physics,* edited by F. Seitz, D. Turnbull, and H. Ehrenreich (Academic, New York, 1966).
[35]J. E. Rowe and D. E. Aspnes, Phys. Rev. Lett. 25, 162 (1970).
[36]Y. P. Varshni, Physica (Utrecht) 34, 149 (1967). The only basis for Varshni's equation is the fact that the gaps should be linear in $T$ at high $T$ and that this dependence should have zero slope at low $T$.
[37]L. Viña, and M. Cardona, Phys. Rev. B 29, 6739 (1984).
[38]H. Richter, Z. P. Wang, and L. Ley, Solid State Commun. 39, 625 (1981).
[39]See, for instance, *Landolt-Börnstein* (new series), edited by O. Madelung (Springer, New York, 1982), Vol. 17a.
[40]D. L. Camphausen, G. A. N. Connell, and W. Paul, Phys. Rev. Lett. 26, 184 (1971).
[41]See, for example, J. B. Theeten and D. E. Aspnes, Ann. Rev. Mater. Sci. 11, 97 (1981).
[42]See, for instance, H. Ehrenreich, in *The Optical Properties of Solids,* edited by J. Tauc (Academic, New York, 1966), p. 106.
[43]M. Cardona, K. L. Shaklee, and F. H. Pollak, Phys. Rev. 154, 696 (1967).
[44]S. M. Kelso, D. E. Aspnes, M. A. Pollak, and R. E. Nahory, Phys. Rev. B 26, 6669 (1982).
[45]W. Hanke, in *Feskörperprobleme (Advances in Solid State Physics),* edited by J. Treusch (Vieweg, Branschweig, 1979), Vol. 19, p. 43.
[46]E. O. Kane, Phys. Rev. 180, 852 (1969); I. Balslev, Solid State Commun. 52, 351 (1984).

[47]M. Cardona, in *Light Scattering in Solids II*, edited by M. Cardona and G. Güntherodt (Springer, New York, 1982).
[48]M. Cardona, Phys. Rev. B **15**, 5999 (1977).
[49]D. E. Aspnes and M. Cardona, Solid State Commun. **27**, 397 (1967).
[50]W. Hanke and L. J. Sham, Phys. Rev. B **21**, 4656 (1980); H. J. Mattausch, W. Hanke, and G. Strinati, *ibid.* **27**, 3735 (1983).
[51]A. Manoogian and A. Leclerc, Can. J. Phys. **57**, 1766 (1979); Phys. Status Solidi B **92**, K23 (1979); A. Manoogian and J. C. Wooley, Can. J. Phys. **62**, 285 (1984).
[52]G. Dresselhaus, A. F. Kipp, and C. Kittel, Phys. Rev. **98**, 368 (1955).
[53]M. Cardona, J. Phys. Chem. Solids **24**, 1543 (1963).
[54]M. Cardona and F. H. Pollak, Phys. Rev. **142**, 530 (1966).
[55]R. A. MacRae, E. T. Arakawa, and M. W. Williams, Phys. Rev. **162**, 615 (1967).
[56]J. N. Hodgson, Proc. Phys. Soc. (London) Sect. B **68**, 593 (1955).
[57]A. I. Golovashkin and G. P. Motulevich, Zh. Eksp. Teor. Fiz. **47**, 64 (1964) [Sov. Phys.—JETP **20**, 44 (1965)].
[58]R. H. W. Graves and A. P. Lenham, J. Opt. Soc. Am. **58**, 884 (1968), and references therein.
[59]See, for example, G. Weisz, Phys. Rev. **149**, 504 (1966).